Acta Cryst E CRYSTALLOGRAPHIC COMMUNICATIONS

ISSN 2056-9890

Crystal structure, Hirshfeld analysis and molecular docking with the vascular endothelial growth factor receptor-2 of (3*Z*)-5-fluoro-3-(hydroxyimino)-indolin-2-one

Bianca Barreto Martins,[a] Leandro Bresolin,[a] Renan Lira de Farias,[b] Adriano Bof de Oliveira[c] and Vanessa Carratu Gervini[a]*

[a]Universidade Federal do Rio Grande (FURG), Escola de Química e Alimentos, Rio Grande, Brazil, [b]Universidade Estadual Paulista (UNESP), Instituto de Química, Araraquara, Brazil, and [c]Universidade Federal de Sergipe (UFS), Departamento de Química, São Cristóvão, Brazil. *Correspondence e-mail: vanessa.gervini@gmail.com

Received 27 May 2017
Accepted 5 June 2017

Edited by C. Rizzoli, Universita degli Studi di Parma, Italy

Keywords: crystal structure; Hirshfeld surface analysis; isatin derivative–VEGFR-2 *in silico* evaluation.

CCDC reference: 1554287

Supporting information: this article has supporting information at journals.iucr.org/e

The reaction between 5-fluoroisatin and hydroxylamine hydrochloride in acidic ethanol yields the title compound, $C_8H_5FN_2O_2$, whose molecular structure matches the asymmetric unit and is nearly planar with an r.m.s. deviation for the mean plane through all non-H atoms of 0.0363 Å. In the crystal, the molecules are linked by N—H···N, N—H···O and O—H···O hydrogen-bonding interactions into a two-dimensional network along the (100) plane, forming rings with $R_2^2(8)$ and $R_1^2(5)$ graph-set motifs. The crystal packing also features weak π–π interactions along the [100] direction [centroid-to-centroid distance 3.9860 (5) Å]. Additionally, the Hirshfeld surface analysis indicates that the major contributions for the crystal structure are the O···H (28.50%) and H···F (16.40%) interactions. An *in silico* evaluation of the title compound with the vascular endothelial growth factor receptor-2 (VEGFR-2) was carried out. The title compound and the selected biological target VEGFR-2 show the N—H···O(*GLU94*), (*CYS96*)N—H···O(isatine) and (*PHE95*)N—H···O(isatine) intermolecular interactions, which suggests a solid theoretical structure–activity relationship.

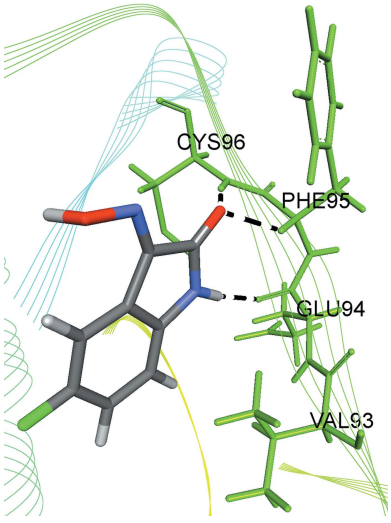

1. Chemical context

The chemistry of isatin is already well documented due to its wide range of applications, especially in organic synthetic chemistry and medicinal chemistry. The first reports on the synthesis of isatin and isatin-based derivatives can be traced back to the first half of the 19th century (Erdmann, 1841*a*,*b*; Laurent, 1841) and almost one hundred years after those publications, the review 'The Chemistry of Isatin' showed the versatility of this molecular fragment (Sumpter, 1944). Two recent examples of this are the synthesis of 1-[(2-methyl-benzimidazol-1-yl) methyl]-2-oxo-indolin-3-ylidene]amino]-thiourea, an *in vitro* and *in silico* Chikungunya virus inhibitor (Mishra *et al.*, 2016) and 5-chloroisatin-4-methylthiosemicarbazone, an intermediate in the HIV-1 (human immunodeficiency virus type 1) RT (reverse transcriptase) inhibitor (Meleddu *et al.*, 2017). For these reasons, the crystal structure determination of isatin-based molecules is an intensive research field and one of our major research aims. Herein, the structure, the Hirshfeld surface analysis and the molecular docking with the vascular endothelial growth factor receptor-2 (VEGFR-2) of the 5-fluoroisatin-3-oxime are reported.

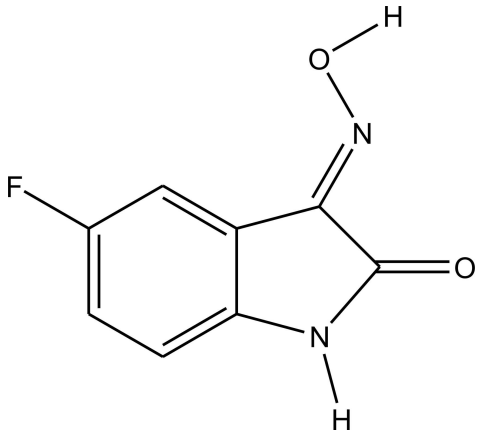

2. Structural commentary

The molecular structure of the title compound (Fig. 1) matches the asymmetric unit and it is nearly planar with an r.m.s. deviation from the mean plane of the non–H atoms of 0.0363 Å [from −0.0806 (9) Å for atom O2 to 0.0575 (11) Å for atom C2]. The C1—C2—N2—O2 and C3—C2—N2—O2 torsion angles are −174.24 (10) and −0.5 (2)°, respectively.

3. Supramolecular features and Hirshfeld surface analysis

In the crystal, the molecules are connected by centrosymmetric pairs of N1—H4···O1^{i} [symmetry code: (i) $-x+1, -y+2, -z+1$] intermolecular interactions into dimers with graph-set motif $R_2^2(8)$ (Table 1). In addition, a remarkable feature consists in an asymmetric bifurcated hydrogen bond with graph-set motif $R_1^2(5)$ involving the H5 atom of the oxime group and the O1^{ii} and N2^{ii} atoms of a neighboring molecule [symmetry code: (ii) $-x+1, y-\frac{1}{2}, -z+\frac{3}{2}$]. These two hydrogen bonds, which form rings with motifs $R_2^2(8)$ and $R_1^2(5)$, connect the molecules into a two-dimensional, tape-like network parallel to the (100) plane. Finally, the molecules are stacked along the [100] direction by weak π–π interactions (Fig. 2) between the benzene and the indolic five-membered rings. The centroid-to-centroid distance is 3.9860 (5) Å).

Table 1
Hydrogen-bond geometry (Å, °).

D—H···A	D—H	H···A	D···A	D—H···A
N1—H4···O1^{i}	0.91 (2)	1.96 (2)	2.8487 (16)	164.7 (18)
O2—H5···N2^{ii}	0.99 (3)	2.69 (2)	3.2989 (16)	120.2 (18)
O2—H5···O1^{ii}	0.99 (3)	1.77 (3)	2.7280 (15)	163 (2)

Symmetry codes: (i) $-x+1, -y+2, -z+1$; (ii) $-x+1, y-\frac{1}{2}, -z+\frac{3}{2}$.

The Hirshfeld surface analysis (Hirshfeld, 1977) of the crystal structure for the title compound was performed. The surface graphical representation, d_{norm}, with transparency and labelled atoms indicates, in magenta colour, the locations of the strongest intermolecular contacts, *e.g.* H4, H5 and O1, which are important for the intermolecular hydrogen bonding (Fig. 3*a*). The Hirshfeld analysis suggests that the major contributions for the crystal packing amount to 25.40% for H···O, 16.40% for H···F and 16.10% for H···H interactions. Other important intermolecular contacts for the cohesion of the structure are (values given in %): C···C = 11.30, H···N = 9.80 and H···C = 6.40 (Wolff *et al.*, 2012; Fig. 4).

4. Comparison with a related structure

For a comparison with the title compound, 5-fluoroisatin-3-oxime, the structure of the related compound 5-chloroisatin-3-

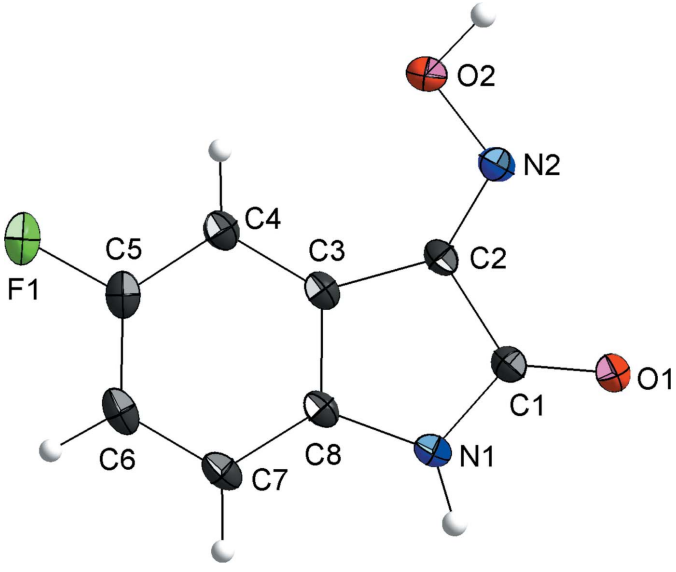

Figure 1
The molecular structure of the title compound with displacement ellipsoids drawn at the 40% probability level.

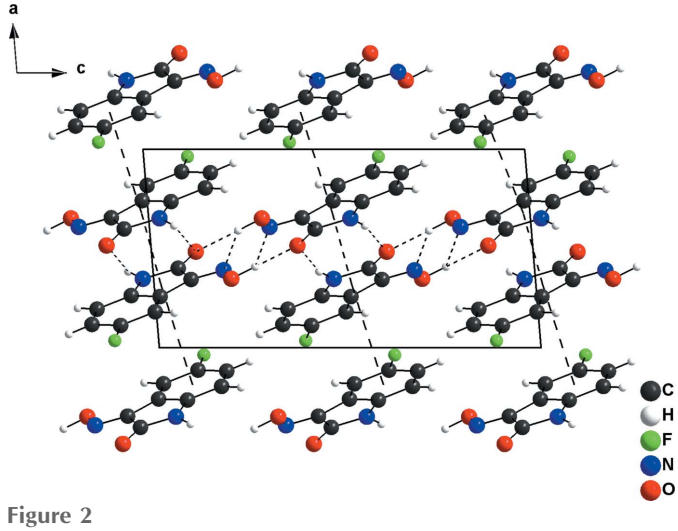

Figure 2
Crystal structure of the title compound viewed along the [010] direction. The H···O and H···N interactions in the crystal packing are shown as dashed lines and connect the molecules into a two-dimensional H-bonded network along the (100) plane. The *Cg*···*Cg* packing along the [100] direction is also shown as dashed lines.

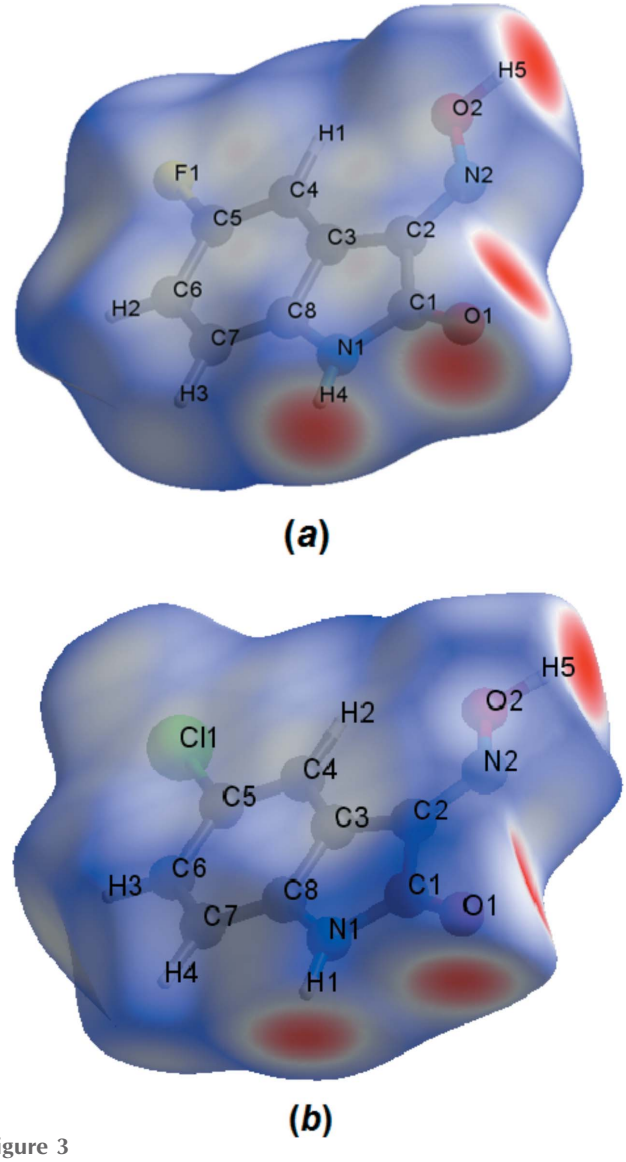

Figure 3
The Hirshfeld surface graphical representation (d_{norm}) for the asymmetric unit of (*a*) the title compound, 5-fluoroisatin-3-oxime, and (*b*) the comparison compound, 5-chloroisatin-3-oxime (Martins *et al.*, 2016). The surface regions with strongest intermolecular interactions are drawn in magenta colour.

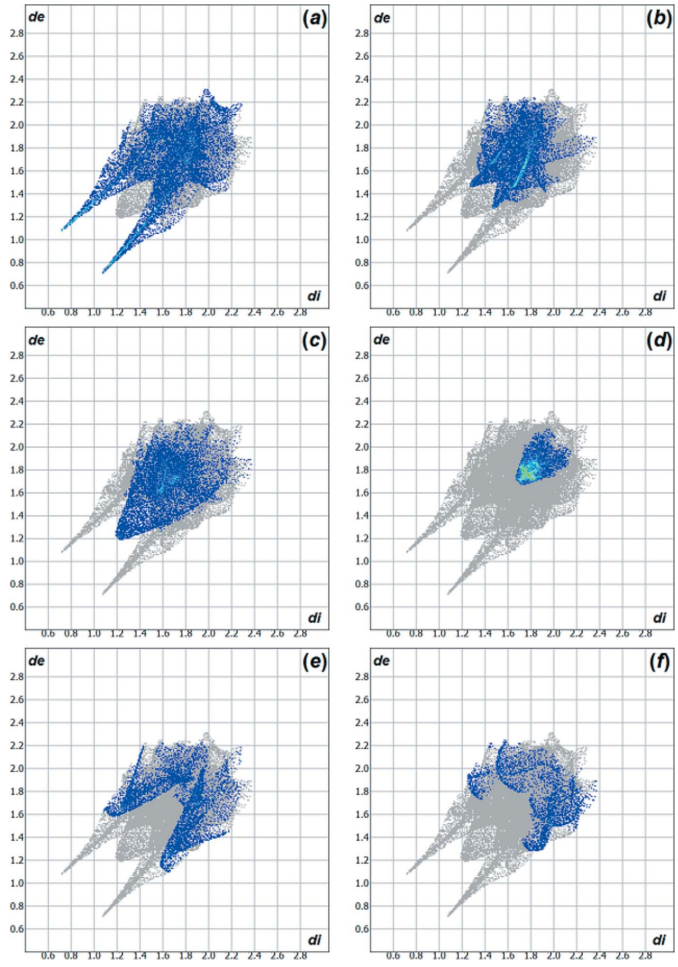

Figure 4
Hirshfeld surface two-dimensional fingerprint plots for the title compound showing the (*a*) H···O, (*b*) H···F, (*c*) H···H, (*d*) C···C, (*e*) H···N and (*f*) H···C contacts in detail (cyan dots). The contributions of the interactions to the crystal packing amount to 25.40%, 16.40%, 16.10%, 11.30%, 9.80% and 6.40%, respectively. The d_e (*y* axis) and d_i (*x* axis) values are the closest external and internal distances (values in Å) from given points on the Hirshfeld surface contacts.

oxime (Martins *et al.*, 2016) was selected. Both structures are nearly planar, build a two-dimensional hydrogen-bonded network parallel to the (100) plane and show the molecules stacked along the [100] direction. The Hirshfeld surface analysis (Hirshfeld, 1977) for 5-chloroisatin-3-oxime was carried out and the Hirshfeld surface graphical representation, d_{norm}, with transparency and labelled atoms indicates, in magenta colour, the locations of the strongest intermolecular contacts, *e.g.* H1, H5 and O1 (Fig. 3*b*). Although the crystal packing (Figs. 2 and 5) and the Hirshfeld surface graphical representations (Fig. 3*a*,*b*) for the title compound and the 5-chloroisatin-3-oxime are quite similar, the contributions of the intermolecular interactions to the cohesion of the crystal structures have differences due to the halogen substituents. For example: for 5-chloroisatin-3-oxime, the H···O interaction amounts to 23.60% and the H···Cl interaction amounts to 18.10%. The contributions to the crystal packing are shown as Hirshfeld surface two-dimensional fingerprint plots with cyan dots. The d_e (*y* axis) and d_i (*x* axis) values are the closest external and internal distances (Å) from given points on the Hirshfeld surface contacts (Figs. 4 and 6; Wolff *et al.*, 2012).

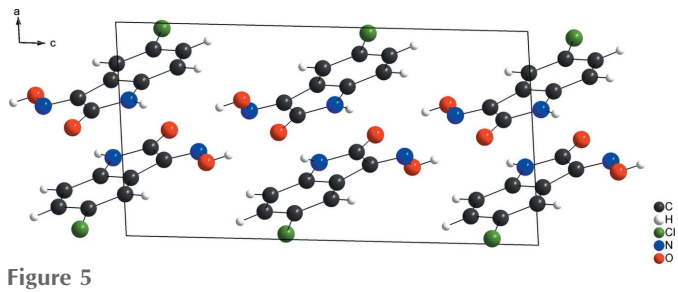

Figure 5
Crystal structure of the comparison compound 5-chloroisatin-3-oxime (Martins *et al.*, 2016), viewed along the [010] direction.

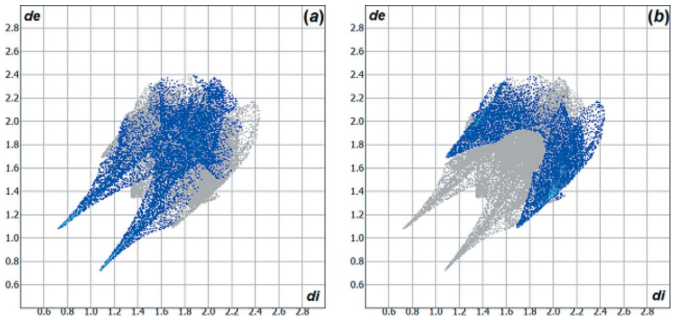

Figure 6
Hirshfeld surface two-dimensional fingerprint plots for the comparison compound 5-chloroisatin-3-oxime (Martins *et al.*, 2016) showing the (*a*) H···O and (*b*) H···Cl contacts in detail (cyan dots). The contributions of the interactions to the crystal packing amount to 23.60% and 18.10%. The d_e (*y* axis) and d_i (*x* axis) values are the closest external and internal distances (values in Å) from given points on the Hirshfeld surface contacts.

5. Molecular docking evaluation

For a lock-and-key supramolecular analysis, a molecular docking evaluation between the title compound and the vascular endothelial growth factor receptor-2 (VEGFR-2) was carried out. Initially, the semi-empirical equilibrium energy of the small molecule was obtained using the PM6 Hamiltonian, but the experimental bond lengths were conserved. The calculated parameters were: heat of formation = −49.353 kJ mol^{-1}, gradient normal = 0.90997, HOMO = −9.265 eV, LUMO = −1.337 eV and energy gap = 7.928 eV (Macrae *et al.*, 2008; Stewart, 2013, 2016). The biological target prediction for the title compound was calculated with the *SwissTargetPrediction* webserver based on the bioisosteric similarity to the isatin entity (Gfeller *et al.*, 2013, 2014). As result of this screening, the title compound showed a promising theoretical structure–activity relationship to kinase proteins sites: 'Frequency Target Class' for kinases amounts to 33% [see the 'SwissTargetPrediction report (5-fluoroisatin-3-oxime)' in the Supporting information]. The protein kinases regulate several critical cellular processes (Wang & Cole, 2014) and the vascular endothelial growth factor receptor-2 kinase inhibition is becoming an attractive subject for anti-cancer drug research (Gao *et al.*, 2015). The crystal structure of the vascular endothelial growth factor receptor-2 (VEGFR-2), PDB ID: 3WZD, was downloaded from Protein Data Bank (Okamoto *et al.*, 2015). Before the calculations, a stereo-chemical evaluation of the protein structure was carried out using the Ramachandran analysis (Lovell *et al.*, 2003) and the number of residues in favoured regions for intermolecular interactions was over 98% [see the 'Number of residues in favoured region (VEGFR-2)' in the Supporting information]. The docking simulation was performed with the *GOLD 5.5* software (Chen, 2015) and a grid of 25 Å was centered on the binding site of Levatinib in the VEGFR-2 kinase (Okamoto *et al.*, 2015). A redocking of the Levatinib compound, an oral multikinase inhibitor that selectively inhibits the vascular endothelial growth factor-2, was used as validation method for the molecular docking protocol (see the 'Re-docking of the Lenvatinib (kinase inhibitor and FDA approved drug)' in the Supporting information]. A calculated global free energy of −20.49 kJ mol^{-1} was found for the title compound and the selected biological target VEGFR-2 interaction and the structure–activity relationship can be assumed by the following observed intermolecular interactions, with the respective hydrogen-bond distances and angles: N—H···O(*GLU94*) [H···O = 2.03 Å, N—H···O = 174°], (*CYS96*)N—H···O(isatine) [H···O = 1.72 Å, N—H···O = 168°] and (*PHE95*)C—H···O(isatine) [H···O = 2.27 Å, C—H···O = 140°] (Fig. 7). Another significant feature of the structure of the title compound is the oxygen atom of the isatin fragment. The O1 atom is a hydrogen-bond acceptor and bridges two D—H···O interactions (supramolecular chemistry, Fig. 2; Hirshfeld surface, Fig. 3; molecular docking with the biological target VEGFR-2 kinase, Fig. 7).

6. Synthesis and crystallization

All starting materials are commercially available and were used without further purification. The synthesis of the title

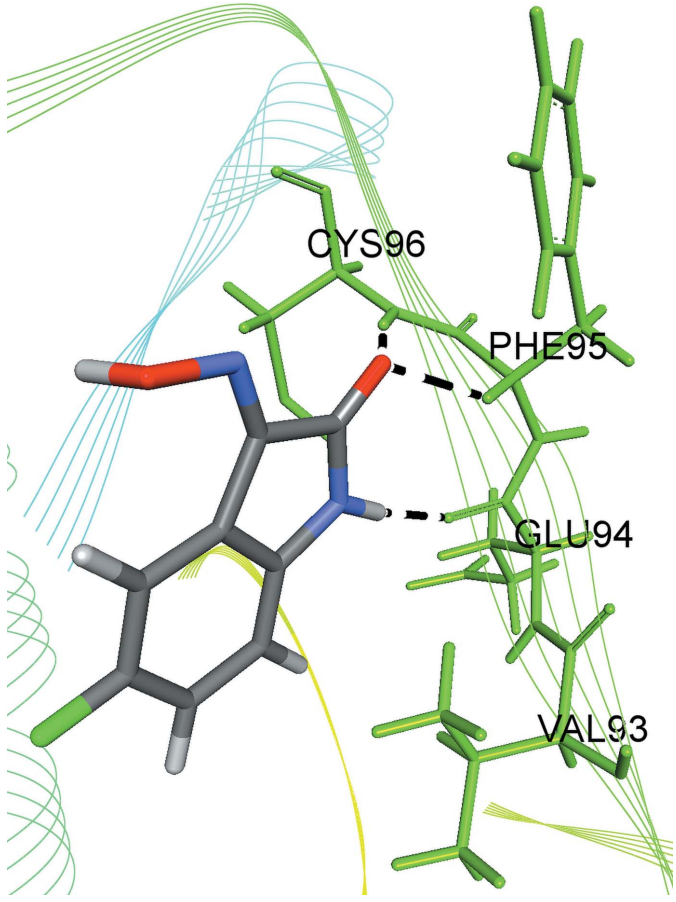

Figure 7
Graphical representation of a lock-and-key model for the intermolecular interactions between the title compound and selected residues of the VEGFR-2. The interactions are shown as dashed lines and the structure of the enzyme is simplified for clarity.

Table 2
Experimental details.

Crystal data	
Chemical formula	$C_8H_5FN_2O_2$
M_r	180.14
Crystal system, space group	Monoclinic, $P2_1/c$
Temperature (K)	200
a, b, c (Å)	7.3036 (10), 7.2045 (10), 14.009 (2)
β (°)	94.736 (4)
V (Å^3)	734.61 (18)
Z	4
Radiation type	Mo $K\alpha$
μ (mm^{-1})	0.14
Crystal size (mm)	0.34 × 0.32 × 0.06
Data collection	
Diffractometer	Bruker APEXII CCD area detector
Absorption correction	Multi-scan (*SADABS*; Krause *et al.*, 2015)
T_{min}, T_{max}	0.663, 0.746
No. of measured, independent and observed [$I > 2\sigma(I)$] reflections	8386, 2142, 1687
R_{int}	0.021
(sin $\theta/\lambda)_{max}$ (Å^{-1})	0.705
Refinement	
$R[F^2 > 2\sigma(F^2)]$, $wR(F^2)$, S	0.040, 0.108, 1.05
No. of reflections	2142
No. of parameters	126
H-atom treatment	H atoms treated by a mixture of independent and constrained refinement
$\Delta\rho_{max}$, $\Delta\rho_{min}$ (e Å^{-3})	0.30, −0.21

Computer programs: *APEX2* and *SAINT* (Bruker, 2014), *SHELXT2014/4* (Sheldrick, 2015*a*), *SHELXL2016/6* (Sheldrick, 2015*b*), *WinGX* (Farrugia, 2012), *DIAMOND* (Brandenburg, 2006), *GOLD* (Chen *et al.*, 2015), *MOPAC* (Stewart, 2016), *CRYSTAL EXPLORER* (Wolff, *et al.*, 2012), *publCIF* (Westrip, 2010) and *enCIFer* (Allen *et al.*, 2004).

compound was adapted from procedures reported previously (Martins *et al.*, 2016; O'Sullivan & Sadler, 1956; Sandmeyer, 1919; Sumpter, 1944). A glacial acetic acid catalyzed mixture of 5-fluoroisatin (3 mmol) and hydroxylamine hydrochloride (3 mmol) in ethanol (50 mL) was stirred and refluxed for 6 h. After cooling and filtering, single crystals suitable for X-ray diffraction were obtained from the ethanolic solution by solvent evaporation.

7. Refinement

Crystal data, data collection and structure refinement details are summarized in Table 2. The H4 and H5 atoms were located in a difference Fourier map and freely refined [N1—H4 = 0.91 (2) Å and O2—H5 = 0.99 (3) Å]. The H1, H2 and H3 atoms were positioned with idealized geometry (HFIX command) and refined using a riding model, with C—H = 0.95 Å and U_{iso}(H) = 1.2U_{eq}(C).

Acknowledgements

ABO is an associate researcher in the project 'Dinitrosyl complexes containing thiol and/or thiosemicarbazone: synthesis, characterization and treatment against cancer', founded by FAPESP, Proc. 2015/12098–0, and acknowledges Professor José C. M. Pereira (São Paulo State University, Brazil) for his support in this work. ABO also acknowledges the VCG for the invitation to be a visiting professor at the Federal University of Rio Grande, Brazil, where part of this work was developed. RLF thanks the CAPES foundation for the scholarship. The authors acknowledge Professor A. J. Bortoluzzi for the access to the experimental facilities and the data collection (Federal University of Santa Catarina, Brazil).

Funding information

Funding for this research was provided by: Coordenação de Aperfeiçoamento de Pessoal de Nível Superior; Conselho Nacional de Desenvolvimento Científico e Tecnológico; Fundação de Amparo à Pesquisa do Estado de São Paulo; Fundação de Amparo à Pesquisa do Estado do Rio Grande do Sul.

References

Allen, F. H., Johnson, O., Shields, G. P., Smith, B. R. & Towler, M. (2004). *J. Appl. Cryst.* **37**, 335–338.
Brandenburg, K. (2006). *DIAMOND*. Crystal Impact GbR, Bonn, Germany.
Bruker (2014). *APEX2* and *SAINT*. Bruker AXS Inc., Madison, Wisconsin, USA.
Chen, Y.-C. (2015). *Trends Pharmacol. Sci.* **36**, 78–95.
Erdmann, O. L. (1841*a*). *Ann. Chim. Phys.* **3**, 355–371.
Erdmann, O. L. (1841*b*). *J. Prakt. Chem.* **22**, 257–299.
Farrugia, L. J. (2012). *J. Appl. Cryst.* **45**, 849–854.
Gao, H., Su, P., Shi, Y., Shen, X., Zhang, Y., Dong, J. & Zhang, J. (2015). *Eur. J. Med. Chem.* **90**, 232–240.
Gfeller, D., Grosdidier, A., Wirth, M., Daina, A., Michielin, O. & Zoete, V. (2014). *Nucleic Acids Res.* **42**, W32–W38.
Gfeller, D., Michielin, O. & Zoete, V. (2013). *Bioinformatics*, **29**, 3073–3079.
Hirshfeld, H. L. (1977). *Theor. Chim. Acta*, **44**, 129–138.
Krause, L., Herbst-Irmer, R., Sheldrick, G. M. & Stalke, D. (2015). *J. Appl. Cryst.* **48**, 3–10.
Laurent, A. (1841). *Ann. Chim. Phys.* **3**, 371–383.
Lovell, S. C., Davis, I. W., Arendall, W. B., de Bakker, P. I., Word, J. M., Prisant, M. G., Richardson, J. S. & Richardson, D. C. (2003). *Proteins*, **50**, 437–450.
Macrae, C. F., Bruno, I. J., Chisholm, J. A., Edgington, P. R., McCabe, P., Pidcock, E., Rodriguez-Monge, L., Taylor, R., van de Streek, J. & Wood, P. A. (2008). *J. Appl. Cryst.* **41**, 466–470.
Martins, B. B., Gervini, V. C., Pires, F. C., Bortoluzzi, A. J. & de Oliveira, A. B. (2016). *IUCrData*, **1**, x161506.
Meleddu, R., Distinto, S., Corona, A., Tramontano, E., Bianco, G., Melis, C., Cottiglia, F. & Maccioni, E. (2017). *J. Enzyme Inhib. Med. Chem.* **32**, 130–136.
Mishra, P., Kumar, A., Mamidi, P., Kumar, S., Basantray, I., Saswat, T., Das, I., Nayak, T. K., Chattopadhyay, S., Subudhi, B. B. & Chattopadhyay, S. (2016). *Sci. Rep.* **6**, 20122.
Okamoto, K., Ikemori-Kawada, M., Jestel, A., von König, K., Funahashi, Y., Matsushima, T., Tsuruoka, A., Inoue, A. & Matsui, J. (2015). *ACS Med. Chem. Lett.* **6**, 89–94.
O'Sullivan, D. G. & Sadler, P. W. (1956). *J. Chem. Soc.* pp. 2202–2207.
Sandmeyer, T. (1919). *Helv. Chim. Acta*, **2**, 234–242.
Sheldrick, G. M. (2015*a*). *Acta Cryst.* A**71**, 3–8.
Sheldrick, G. M. (2015*b*). *Acta Cryst.* C**71**, 3–8.
Stewart, J. J. P. (2013). *J. Mol. Model.* **19**, 1–32.
Stewart, J. J. P. (2016). *MOPAC2016*. Stewart Computational Chemistry, Colorado Springs, Colorado, United States of America.

Sumpter, W. C. (1944). *Chem. Rev.* **34**, 393–434.
Wang, Z. & Cole, P. A. (2014). *Methods Enzymol.* **548**, 1–21.
Westrip, S. P. (2010). *J. Appl. Cryst.* **43**, 920–925.
Wolff, S. K., Grimwood, D. J., McKinnon, J. J., Turner, M. J., Jayatilaka, D. & Spackman, M. A. (2012). *CRYSTAL EXPLORER*. University of Western Australia, Perth, Australia.

supporting information

Acta Cryst. (2017). E**73**, 987-992 [https://doi.org/10.1107/S2056989017008301]

Crystal structure, Hirshfeld analysis and molecular docking with the vascular endothelial growth factor receptor-2 of (3*Z*)-5-fluoro-3-(hydroxyimino)-indolin-2-one

Bianca Barreto Martins, Leandro Bresolin, Renan Lira de Farias, Adriano Bof de Oliveira and Vanessa Carratu Gervini

Computing details

Data collection: *APEX2* (Bruker, 2014); cell refinement: *SAINT* (Bruker, 2014); data reduction: *SAINT* (Bruker, 2014); program(s) used to solve structure: *SHELXT2014/4* (Sheldrick, 2015a); program(s) used to refine structure: *SHELXL2016/6* (Sheldrick, 2015b), *WinGX* (Farrugia, 2012); molecular graphics: *DIAMOND* (Brandenburg, 2006), *GOLD* (Chen *et al.*, 2015), *MOPAC* (Stewart, 2016), *CRYSTAL EXPLORER* (Wolff, *et al.*, 2012); software used to prepare material for publication: *publCIF* (Westrip, 2010), *enCIFer* (Allen *et al.*, 2004).

(3*Z*)-5-Fluoro-3-(hydroxyimino)indolin-2-one

Crystal data

$C_8H_5FN_2O_2$
M_r = 180.14
Monoclinic, $P2_1/c$
a = 7.3036 (10) Å
b = 7.2045 (10) Å
c = 14.009 (2) Å
β = 94.736 (4)°
V = 734.61 (18) Å^3
Z = 4
$F(000)$ = 368
D_x = 1.629 Mg m^{-3}
Mo $K\alpha$ radiation, λ = 0.71073 Å
Cell parameters from 3387 reflections
θ = 2.8–30.0°
μ = 0.14 mm^{-1}
T = 200 K
Plate, yellow
0.34 × 0.32 × 0.06 mm

Data collection

Bruker APEXII CCD area detector diffractometer
Radiation source: fine-focus sealed X-ray tube
φ and ω scans
Absorption correction: multi-scan (SADABS; Krause *et al.*, 2015)
T_{min} = 0.663, T_{max} = 0.746
8386 measured reflections
2142 independent reflections
1687 reflections with $I > 2\sigma(I)$
R_{int} = 0.021
θ_{max} = 30.1°, θ_{min} = 2.8°
h = −10→10
k = −10→7
l = −19→19

Refinement

Refinement on F^2
Least-squares matrix: full
$R[F^2 > 2\sigma(F^2)]$ = 0.040
$wR(F^2)$ = 0.108
S = 1.05
2142 reflections
126 parameters
0 restraints
Primary atom site location: structure-invariant direct methods

Secondary atom site location: difference Fourier map	$w = 1/[\sigma^2(F_o^2) + (0.0428P)^2 + 0.3741P]$ where $P = (F_o^2 + 2F_c^2)/3$
Hydrogen site location: mixed	$(\Delta/\sigma)_{max} < 0.001$
H atoms treated by a mixture of independent and constrained refinement	$\Delta\rho_{max} = 0.30$ e Å^{-3}
	$\Delta\rho_{min} = -0.21$ e Å^{-3}

Special details

Geometry. All esds (except the esd in the dihedral angle between two l.s. planes) are estimated using the full covariance matrix. The cell esds are taken into account individually in the estimation of esds in distances, angles and torsion angles; correlations between esds in cell parameters are only used when they are defined by crystal symmetry. An approximate (isotropic) treatment of cell esds is used for estimating esds involving l.s. planes.

Fractional atomic coordinates and isotropic or equivalent isotropic displacement parameters (Å²)

	x	*y*	*z*	U_{iso}*/U_{eq}
C1	0.40095 (17)	0.78184 (19)	0.56663 (9)	0.0247 (3)
C2	0.34449 (16)	0.59266 (19)	0.59782 (9)	0.0225 (3)
C3	0.25830 (15)	0.49961 (19)	0.51303 (8)	0.0219 (3)
C4	0.18138 (17)	0.3250 (2)	0.49698 (10)	0.0263 (3)
H1	0.176175	0.236360	0.546869	0.032*
C5	0.11244 (18)	0.2879 (2)	0.40349 (10)	0.0297 (3)
C6	0.11742 (18)	0.4116 (2)	0.32854 (10)	0.0306 (3)
H2	0.068596	0.377653	0.266022	0.037*
C7	0.19449 (18)	0.5867 (2)	0.34516 (9)	0.0277 (3)
H3	0.199749	0.674448	0.294847	0.033*
C8	0.26306 (16)	0.62779 (19)	0.43768 (9)	0.0227 (3)
F1	0.03607 (14)	0.11739 (14)	0.38491 (7)	0.0459 (3)
N1	0.34730 (16)	0.79375 (17)	0.47154 (8)	0.0261 (3)
N2	0.39084 (15)	0.54652 (17)	0.68513 (8)	0.0262 (3)
O1	0.48449 (15)	0.90064 (15)	0.61615 (7)	0.0324 (3)
O2	0.34792 (15)	0.36593 (15)	0.70338 (7)	0.0340 (3)
H4	0.384 (3)	0.889 (3)	0.4351 (15)	0.046 (5)*
H5	0.409 (3)	0.352 (3)	0.7684 (18)	0.073 (7)*

Atomic displacement parameters (Å²)

	U^{11}	U^{22}	U^{33}	U^{12}	U^{13}	U^{23}
C1	0.0267 (6)	0.0261 (7)	0.0210 (6)	0.0027 (5)	0.0005 (4)	−0.0002 (5)
C2	0.0219 (5)	0.0254 (7)	0.0201 (6)	0.0032 (5)	0.0008 (4)	−0.0008 (5)
C3	0.0190 (5)	0.0268 (7)	0.0197 (5)	0.0034 (5)	0.0007 (4)	−0.0020 (5)
C4	0.0241 (6)	0.0297 (7)	0.0249 (6)	0.0013 (5)	0.0013 (4)	−0.0016 (5)
C5	0.0261 (6)	0.0307 (8)	0.0318 (7)	−0.0015 (5)	−0.0006 (5)	−0.0086 (6)
C6	0.0262 (6)	0.0418 (9)	0.0230 (6)	0.0020 (6)	−0.0030 (5)	−0.0077 (6)
C7	0.0248 (6)	0.0375 (8)	0.0202 (6)	0.0031 (5)	−0.0013 (4)	0.0005 (5)
C8	0.0197 (5)	0.0280 (7)	0.0203 (6)	0.0037 (5)	0.0006 (4)	−0.0008 (5)
F1	0.0545 (6)	0.0398 (6)	0.0416 (5)	−0.0143 (4)	−0.0063 (4)	−0.0097 (4)
N1	0.0310 (5)	0.0262 (6)	0.0204 (5)	−0.0006 (5)	−0.0023 (4)	0.0032 (4)
N2	0.0293 (5)	0.0279 (6)	0.0214 (5)	0.0006 (4)	0.0010 (4)	0.0018 (4)
O1	0.0454 (6)	0.0279 (6)	0.0230 (5)	−0.0052 (4)	−0.0025 (4)	−0.0014 (4)

O2	0.0434 (6)	0.0314 (6)	0.0263 (5)	−0.0062 (4)	−0.0029 (4)	0.0069 (4)

Geometric parameters (Å, º)

C1—O1	1.2313 (16)	C5—C6	1.380 (2)
C1—N1	1.3599 (16)	C6—C7	1.393 (2)
C1—C2	1.4994 (19)	C6—H2	0.9500
C2—N2	1.2857 (16)	C7—C8	1.3825 (18)
C2—C3	1.4605 (17)	C7—H3	0.9500
C3—C4	1.3883 (19)	C8—N1	1.4089 (18)
C3—C8	1.4051 (18)	N1—H4	0.91 (2)
C4—C5	1.3898 (19)	N2—O2	1.3674 (16)
C4—H1	0.9500	O2—H5	0.99 (3)
C5—F1	1.3651 (17)		
O1—C1—N1	126.68 (13)	C5—C6—C7	119.57 (12)
O1—C1—C2	127.09 (12)	C5—C6—H2	120.2
N1—C1—C2	106.19 (11)	C7—C6—H2	120.2
N2—C2—C3	135.81 (13)	C8—C7—C6	117.44 (13)
N2—C2—C1	117.07 (12)	C8—C7—H3	121.3
C3—C2—C1	106.90 (10)	C6—C7—H3	121.3
C4—C3—C8	120.57 (12)	C7—C8—C3	122.27 (13)
C4—C3—C2	133.56 (12)	C7—C8—N1	127.72 (13)
C8—C3—C2	105.88 (12)	C3—C8—N1	110.00 (11)
C3—C4—C5	115.94 (13)	C1—N1—C8	111.02 (11)
C3—C4—H1	122.0	C1—N1—H4	121.6 (13)
C5—C4—H1	122.0	C8—N1—H4	126.2 (13)
F1—C5—C6	118.18 (12)	C2—N2—O2	112.17 (11)
F1—C5—C4	117.62 (14)	N2—O2—H5	100.2 (15)
C6—C5—C4	124.20 (14)		
O1—C1—C2—N2	−1.5 (2)	C5—C6—C7—C8	−0.05 (19)
N1—C1—C2—N2	176.30 (12)	C6—C7—C8—C3	0.59 (19)
O1—C1—C2—C3	−176.99 (13)	C6—C7—C8—N1	179.71 (12)
N1—C1—C2—C3	0.84 (13)	C4—C3—C8—C7	−0.73 (18)
N2—C2—C3—C4	5.3 (2)	C2—C3—C8—C7	179.29 (11)
C1—C2—C3—C4	179.49 (13)	C4—C3—C8—N1	−179.98 (11)
N2—C2—C3—C8	−174.73 (14)	C2—C3—C8—N1	0.04 (14)
C1—C2—C3—C8	−0.53 (13)	O1—C1—N1—C8	177.00 (13)
C8—C3—C4—C5	0.28 (18)	C2—C1—N1—C8	−0.83 (14)
C2—C3—C4—C5	−179.75 (13)	C7—C8—N1—C1	−178.67 (12)
C3—C4—C5—F1	179.86 (11)	C3—C8—N1—C1	0.53 (15)
C3—C4—C5—C6	0.3 (2)	C3—C2—N2—O2	−0.5 (2)
F1—C5—C6—C7	−179.98 (12)	C1—C2—N2—O2	−174.24 (10)
C4—C5—C6—C7	−0.4 (2)		

Hydrogen-bond geometry (Å, º)

D—H···*A*	*D*—H	H···*A*	*D*···*A*	*D*—H···*A*
N1—H4···O1^{i}	0.91 (2)	1.96 (2)	2.8487 (16)	164.7 (18)
O2—H5···N2^{ii}	0.99 (3)	2.69 (2)	3.2989 (16)	120.2 (18)
O2—H5···O1^{ii}	0.99 (3)	1.77 (3)	2.7280 (15)	163 (2)

Symmetry codes: (i) −*x*+1, −*y*+2, −*z*+1; (ii) −*x*+1, *y*−1/2, −*z*+3/2.